Applied Catalysis B: Environmental 339 (2023) 123092

Contents lists available at ScienceDirect

Applied Catalysis B: Environmental

journal homepage: www.elsevier.com/locate/apcatb

Strong influence of the heating method on Ti/RuO_2-TiO_2 anode electrochemical and photoassisted electrochemical performance

Aline R. Dória [a,b,c], Isabelle M.D. Gonzaga [a,b,c], Gessica O.S. Santos [a,b,c], Caio V.S. Almeida [a,b], Deyvid C. Silva [d], Ronaldo S. Silva [d], Luciane P.C. Romão [e], Cristina Sáez [e], Giancarlo R. Salazar-Banda [a,b,*], Katlin I.B. Eguiluz [a,b,*]

[a] Electrochemistry and Nanotechnology Laboratory, Institute of Technology and Research (ITP), 49032–490 Aracaju, SE, Brazil
[b] Graduate Program in Process Engineering (PEP), Universidade Tiradentes, 49032–490 Aracaju, SE, Brazil
[c] Chemical Engineering Department, Faculty of Chemical Sciences and Technologies, University of Castilla-La Mancha, Enrique Costa Novella Building, Campus Universitario s/n, 13071 Ciudad Real, Spain
[d] Functional Nanomaterials Group, Department of Physics, Federal University of Sergipe, São Cristóvão, SE, Brazil
[e] Study of Natural Organic Matter Laboratory, Federal University of Sergipe, 49100–000 São Cristovão, SE, Brazil

ARTICLE INFO

Keywords:
Ciprofloxacin
Electrooxidation
Hypochlorite evolution
Mineralization

ABSTRACT

The use of mixed metal oxide anodes in wastewater electrochemical treatment depends on the production of efficient, stable, and economically viable anodes. Thus, Ti/RuO_2-TiO_2 anodes were prepared by unconventional heating methods using a CO_2 laser and microwave irradiation. The calcination method significantly modified the surface morphology, electronic structure, and electrocatalytic properties of the anodes. Compared with the conventionally-prepared anode, anodes made using laser and microwave display increase by approximately 2 and 3 times the voltammetric charge and decrease by 2.8 and 5.4 times the charge transfer resistance. Moreover, laser and microwave-prepared anodes presented a lifetime of 4.4 and 2.3 times longer than the furnace-prepared anode. High efficiency in generating hypochlorite is achieved in 1 h using a laser-prepared anode (372 mg L^{-1}), which improves the degradation and mineralization of ciprofloxacin by electrolysis. After UVC-irradiation, the anode with the lowest energy consumption (7.14 kWh g^{-1}TOC) was prepared by microwave radiation.

1. Introduction

Worldwide technological growth and continuous industrialization have given rise to many industrial effluents carrying complex organic pollutants into the environment. These contaminants can cause significant harm to human health and the environment since most of these chemical pollutants are persistent and toxic to conventional biological wastewater treatments [1]. The abundant use and disposal of pharmaceutical and personal care products resulted in the recurrent detection of these compounds in effluents even after being processed in wastewater treatment plants. A worrisome fact is its persistence in the environment and low biodegradability [2,3].

Ciprofloxacin (CIP) is an important antibiotic of the fluoroquinolone class for treating human and animal diseases. As with most antibiotics, large percentages of CIP are excreted unmetabolized. As a result, this organic compost often enters the environment by the discharge of untreated sewage, wastewater, manure stocks from confined animal feeding operations, and runoff from farmland into nearby streams. CIP is among the top ten emerging high-priority contaminants, and its presence in wastewater and surface water, even in low concentrations, is considered an environmental hazard. The concentration of CIP measured near drug factories is up to 50 mg L^{-1}, whereas in wastewater and surface water effluents, it varies from ng L^{-1} to mg L^{-1} [3,4]. Hence, developing more effective and versatile technologies is essential for treating these pollutants and controlling water pollution. Among the existing technologies, electrochemical processes are very promising for degrading organic compounds in aqueous media, as they present compact, easily scalable, and automatable systems [1,5,6].

The effectiveness and performance of electrochemical processes largely depend on the properties of the anodic materials [7–9]. Parameters involved during coating preparation, such as solvent, precursor solution preparation, calcination temperature, coating deposition, and annealing atmosphere, are known to influence the physical and electrochemical properties of coatings [10–13]. Our research group has been

* Corresponding authors at: Electrochemistry and Nanotechnology Laboratory, Institute of Technology and Research (ITP), 49032–490 Aracaju, SE, Brazil.
E-mail addresses: giancarlo.richard@souunit.com.br (G.R. Salazar-Banda), katlin.ivon@souunit.com.br (K.I.B. Eguiluz).

https://doi.org/10.1016/j.apcatb.2023.123092
Received 29 June 2022; Received in revised form 30 April 2023; Accepted 9 July 2023
Available online 11 July 2023

striving to improve the synthesis conditions of mixed metal oxide (MMO) anodes, seeking the improvement of some properties, especially the stability of these materials [11,14–19]. Currently, MMOs have been prepared by different heating methods, including CO_2 laser and microwave heating [10,14,17,18,20]. The electrochemical properties and stability of MMOs prepared using these methods can be improved. For example, anodes of Ti/RuO_2-IrO_2 prepared by laser [17] and microwave [14] heating presented a service lifetime of 1.6 and 3.5 times longer than those manufactured conventionally in electric furnaces.

Ruthenium-based MMOs have been explored for a wide range of applications, mainly ruthenium and iridium mixture; however, these metal oxides are very expensive [21]. Alternatively, titanium dioxide (TiO_2)-based MMOs have been widely used due to their cost-effectiveness (desirable properties as electrodes, such as semiconductor character, excellent electrocatalytic and photoelectrocatalytic activity, and low cost) [21]. Pure oxide has insulating behavior, so the combination of TiO_2 with noble metal oxides is required to produce suitable anodes for electrochemical [22] and photoassisted electrochemical applications [23]. In recent studies, RuO_2/TiO_2 heterojunctions have been developed for photocatalytic and photoelectrocatalytic processes [24,25]. For example, Uddin et al. conducted impregnation of TiO_2 nanoparticles with ruthenium(III) 2,4-pentanedionate to form RuO_2/TiO_2 particles, which in turn showed both anatase and rutile phases, showing improved performance in the degradation of methylene blue [25]. In another approach, a recent study reported the influence of ruthenium doping TiO_2 nanotube arrays. The Ru-doped TiO_2 photoanode presented improved performance towards decolorization of Terasil Blue dye under UV or visible light. In that study, the predominance of the anatase phase over the rutile one and the positive effect of doping on visible-light photoactivity were demonstrated [26]. However, TiO_2 used in MMO synthesis is commonly present in the rutile phase, which does not show photoactivity [27].

In this sense, the improvement of the physical and electrochemical properties of Ti/RuO_2-TiO_2 anodes prepared using laser heating has already been reported in a previous study [10], whereas the use of microwave heating for this anode composition has yet to be reported. Likewise, the influence of the heating method used during the synthesis of Ti/RuO_2-TiO_2 anodes on their physical properties and electrochemical performance is still unknown. Additionally, its stability and applicability for the electrochemical treatment (alone or combined with other methods) of effluents contaminated with organic compounds should be investigated.

Based on these gaps, we report the synthesis and characterization of Ti/RuO_2-TiO_2 anodes using a CO_2 laser, microwave heating, and an electric furnace. The prepared materials were characterized physically and electrochemically. Additionally, the synergistic/antagonistic effects resulting from the coupling of electrochemical oxidation (EC) with UVC light irradiation (electrochemical photoassisted, PhEC) for the removal of ciprofloxacin (model pollutant) using the differently prepared anodes were evaluated.

2. Experimental section

2.1. Chemicals and electrode materials

All chemical reagents used were of analytical grade and were used without further purification. Citric acid (99.5%) and isopropyl alcohol (99.5%) were acquired from Vetec®. Ethylene glycol (99.8%), ruthenium (III) chloride (99.5%), titanium (IV) butoxide (97%), oxalic acid (99.5%), sodium chloride (99.9%), acetonitrile (99.9%), ciprofloxacin (98%) and sulfuric acid (95.0–98.0%) were purchased from Sigma–Aldrich®. Hydrochloric acid (38.0%) is from Synth®. All solutions were prepared with ultrapure water from a Gehaka Master All 2000 System (18.2 MΩ cm, 25 °C).

2.2. Preparation of the MMO anodes

The anodes were obtained by coating a titanium substrate with $(RuO_2)_{30}(TiO_2)_{70}$. Initially, the precursor solution was prepared using the Pechini method with ethylene glycol:citric acid:metal molar ratio of 10:3:1 [10]. Initially, ethylene glycol was heated to 60 °C, and citric acid was added. After complete dissolution, the metallic precursors added were ruthenium (III) chloride and titanium (IV) butoxide. The precursor solution was applied by brushing onto a previously pretreated titanium substrate (pretreatment was described by Santos et al. [15]). After brushing, the anodes were submitted to a heating treatment using three different methods: the conventional heating method, a CO_2 laser (GEM-100 L - Coherent) as the only heating source operating in continuous mode, and hybrid microwave heating. The microwave used for heating is from the Consul brand, with a capacity of 20 L, operating with a maximum power of 700 W and a frequency of 2.45 GHz. A box of insulating bricks was built to carry out hybrid heating, and SiC plates (susceptors) with a high dielectric constant (9.7) were placed inside this box [14]. The coating and calcination steps were repeated until the anodes reached a mass of deposited oxides of 1.2 mg cm^{-2}. Fig. SM1 shows a representative schematic of anode production by different heating methods.

The preparation of anodes in a furnace (EDG 3 P muffle model 3000) followed the following calcination steps: 130 °C for 30 min, 250 °C for 10 min, and the desired temperature for 5 min at a heating rate of 5 °C min^{-1}. After reaching the desired mass, the final calcination was performed for 60 min [15]. The coated titanium was positioned below the circular laser beam operating continuously and kept fixed under the electrode area of 1 cm^2 to prepare the CO_2 laser-made anode. A focal length of 27 cm was used [17]. After reaching the desired temperature, the heating was turned off after 40 s [10]. Finally, the irradiation was continuously applied to the electrodes prepared by microwave hybrid heating until it reached the desired temperature. Once this temperature was reached, the equipment was turned off. The final calcination temperature for all anodes was 400 °C.

2.3. Characterization of the MMO anode

2.3.1. Physical characterization

X-ray diffraction (XRD) patterns were recorded using a PANalytical Empyrean diffractometer in the 2θ range from 20° to 80° and Cu Kα radiation (λ = 1.5418 nm) at 40 kV and 40 mA. The measurements were performed in two ways: In the first (supplementary material), the measurements were done in continuous mode with a scanning speed of 2 min^{-1} to compare the coverage of the film; The second was carried out in step-scan mode and only using the RuO_2-TiO_2 powder after its removal from the Ti substrate. This procedure was important to perform the Rietveld refinement of the diffractograms eliminating the metallic Ti peaks from the substrate. The Rietveld refinement was carried out using X'pert High Score Plus software. The top view morphologies and the elemental mapping were observed using a scanning electron microscope (SEM, JEOL JSM-6510LV). X-ray photoelectron spectroscopy (XPS) measurements were performed using an Omicron (CHA - Concentric Hemisferica Analyser) spectrometer with monochromatic Al Kα X-ray source radiation ($h\nu = 1486.6$ eV) at a base pressure of 5×10^{-9} mbar. The spectra were deconvoluted using the CasaXPS software Levenberg–Marquardt algorithm. The binding energies of the spectra were referenced against the C 1 s component of adventitious carbon at 284.6 eV. Peak energies are given with an accuracy of 0.1 eV. The bandgap energy of the catalysts was determined by diffuse reflectance spectroscopy (DRS) performed using a Shimadzu UV-2600 UV—Vis spectrophotometer in the 200–700 nm wavelength range.

2.3.2. Electrochemical characterization

The MMO anodes were electrochemically characterized in a conventional three-electrode glass cell configured for three electrodes, with

a Pt electrode (2 cm^2) as the counter electrode, an Ag/AgCl electrode as the reference electrode, and the MMO anodes as the working electrode (2 cm^2). All electrochemical characterization tests were carried out on an Autolab PGSTAT302N (Metrohm – Pensalab) using 80 mL of a 0.5 mol L^{-1} H_2SO_4 aqueous solution as the electrolyte.

Cyclic voltammetry experiments with the synthesized Ti/RuO_2-TiO_2 electrodes were conducted from 0.0 to 1.2 V at a scan rate of 50 mV s^{-1}. The morphology factor was calculated using the total differential capacitance ($C_{d,t}$), internal differential capacitance ($C_{d,i}$), and external differential capacitance ($C_{d,e}$), as proposed by Silva et al. [28]. The oxygen evolution potential (OEP) for the synthesized anodes was measured by linear scanning at 10 mV s^{-1}. The potentials corresponding to the inflection point of the linear polarization curves were defined as the oxygen evolution onset potential [29]. Electrochemical impedance spectroscopy (EIS) analyses were carried out over the frequency range from 100 kHz to 10 mHz. The imposed AC amplitude was 5 mV s^{-1}. Accelerated life tests (ALT) were performed to evaluate the stability of the anodes. The constant current density used for ALT was 500 mA cm^{-2}. Deactivation of the electrode was considered when the cell voltage reached 10 V.

2.3.3. Chlorine speciation and degradation of ciprofloxacin in irradiated and nonirradiated processes

Bench-scale electrolysis and electrolysis photoassisted were carried out under galvanostatic conditions to determine the influence of the preparation method of the anodes on the electrochemical generation of hypochlorite and the electrochemical degradation of ciprofloxacin (CIP). The same electrochemical cell used in the electrochemical characterization of the anodes was used for these experiments. The synthesized RuO_2-TiO_2 anodes, with a geometric area of 2 cm^2, were used as anode materials and stainless steel AISI 304 was used as the cathode (2 cm^2). The current density was 30 mA cm^{-2} for 2 h, and 100 mL of a 3.7 g L^{-1} (0.06 mol L^{-1}) NaCl solution was used as a supporting electrolyte. The initial concentration of the CIP pollutant was 50 mg L^{-1} for both electrochemical and electrochemical photoassisted oxidation. Electrochemical photoassisted experiments were carried out by immersing a 9 W UV-C lamp (254 nm, brand Anself) in the bulk solution.

The concentration of HClO (predominant specie formed at pH 3 −7) was determined as ClO^- after the addition of 50 uL of 3 M NaOH in a 3 mL sample employing the spectrophotometric method (λ = 293 nm) using a UV—Vis spectrophotometer (model UV-M51, Bel Photonics). The anions chlorate and perchlorate were measured by ions chromatography (Metrohm) using a Metrosep A Supp 5 column (150 mm × 4.0 mm). The mobile phase consisted of 3.2 mM Na_2CO_3 and 1 mM $NaHCO_3$ solutions in water at a flow rate of 0.7 mL min^{-1} and 25 °C. The ciprofloxacin concentration was measured using Shimadzu Prominence HPLC equipment coupled with a diode array detector (DAD) at 254 nm. A reversed-phase C18 column (model Kinetex, Phenomenex) (250 mm × 4.6 mm, 5 μm - particle size) was used. The mobile phase consisted of 50% ultrapure water (phase A) and 50% acetonitrile (phase B) in isocratic mode. The flow was 0.5 mL min^{-1}, the injection volume was 25 μL, the run time was 10 min, the ciprofloxacin retention time was 5.7 min, and the oven temperature was 40 °C.

The kinetic model used was the pseudo-first-order ($C/C_0 = e^{-kt}$), where C (mg L^{-1}) is the residual CIP concentration at time t (min), C_0 (mg L^{-1}) is the initial CIP concentration, and k (min^{-1}) is the pseudo-first-rate constant order. The goodness of fit of the model to the data was evaluated through the linear correlation coefficient (R^2).

The total organic carbon (TOC) analyses were performed on a Shimadzu TOC analyzer, model TOC-V CPH. The energy consumption per unit mass of TOC removed (EC_{TOC}, kW h g^{-1}) after the treatment time was calculated according to the following equation:

$$EC_{TOC}(\text{kW h g}^{-1}\text{TOC}) = \frac{(U \times I \times t) + (P_{lamp}\, x\, t)}{V_s \times \Delta_{TOC}} \quad (1)$$

where U is the measured cell potential (V) at the given treatment time, P_{lamp} is the power of the lamp (W), and V_s (L) is the treated volume.

3. Results and discussion

3.1. Processing time

Some aspects need to be studied for the practical application of novel materials, including their synthesis method. In particular, anodes prepared using thermal decomposition methods require the application of several coating layers, which vary according to the desired mass density and composition. Here, seven heating and cooling steps were performed to prepare Ti/RuO_2-TiO_2 anodes using the conventional furnace and unconventional heating methods (laser and microwave), thus obtaining 1.2 mg cm^{-2} of the oxides on the Ti substrate. According to the methodology already described by our group [7], in the preparation of this MMO anode in a furnace, the heating time of each layer is 2.1 h. Later, the furnace is turned off, and the material remains inside until it reaches room temperature (nearly 4.2 h). For microwave heating, approximately 0.47 h is required to attain the desired temperature in each layer, while the cooling time is approximately 1 h. Interestingly, the layering time using laser heating is ultrafast (i.e., 40 s), while cooling occurs almost instantaneously. Therefore, the total time for producing anodes prepared by heating in a furnace, microwave, and laser was 43.8 h, 10.3 h, and 0.1 h, respectively (Fig. SM2). Hence, the unconventional heating methods significantly reduce the production time by approximately 438 and 4.25 times.

3.2. Physical characterization

XPS measurements were used to determine the chemical composition of the surface of the Ti/$Ru_{0.3}Ti_{0.7}O_2$ anodes. Apart from a C 1 s peak located at approximately 284.6 eV, which might be attributed to the adventitious carbon-based contaminant [30], the survey scans (Fig. SM3) of the anodes only detected emissions related to titanium, oxygen, and ruthenium, as expected. The XPS full spectra showed a superposition of the adventitious carbon C 1 s peak with the Ru 3d signal and the Ru $3p_{3/2}$ with the Ti 2p peaks. The Ru 3p1/2 peak was used to quantify the Ru composition instead of the 3d peak to avoid interferences from the carbon signal. Table 1 provides the elemental composition of the anodes under study obtained by XPS.

Table 1 confirms the presence of Ti as the most prominent metal on all anodes. However, it is noteworthy that the atomic percentage of Ru found for the anode prepared using the microwave heating method was almost twice that observed for the other methods. The different amounts of Ru on the surface of the electrodes may result in different electrochemical behaviors of these materials, which will be investigated later.

The O 1 s core-level spectra for the Ti/$Ru_{0.3}Ti_{0.7}O_2$ anodes (Fig. SM4) were deconvoluted into three peaks. The most prominent peak was attributed to the M−O bond (M = Ru and Ti), indicating the formation of

Table 1
Elemental composition of the anodes under study obtained from XPS.

Heating method	Elements	Atomic %
Furnace	C	40.8
	O	43.8
	Ru*	2.33
	Ti	13.1
Laser	C	40.3
	O	45.8
	Ru*	2.66
	Ti	11.2
Microwave	C	42.9
	O	43.0
	Ru*	4.15
	Ti	9.96

* Obtained from Ru 3p1/2 peak

metal oxides [31]. The other peaks can be related to the O−H species adsorbed onto the surface of the anodes and M−O−H groups [31].

Fig. 1 presents the deconvoluted Ti 2p high-resolution spectra taken for the $Ti/Ru_{0.3}Ti_{0.7}O_2$ anodes, which coincide with the Ru $3p_{3/2}$ peak. The Ti 2p spectrum of the anode prepared through the conventional method, i.e., in the furnace (Fig. 1a), showed Ti $2p_{3/2}$ and Ti $2p_{1/2}$ peaks at 459.8 and 465.5 eV, respectively, consistent with the Ti^{4+} oxidation state. The spin-orbit splitting was 5.7 eV for all anodes, which agrees with the expected Ti^{4+} oxidation state in the TiO_2 species [32–34].

Interestingly, as shown in Fig. 1d, the XPS spectra of the anodes prepared by the laser (Fig. 1b) and microwave methods (Fig. 1c) displayed a 1.9 and 1.7 eV shift of the Ti 2p signal toward lower binding energies. The observed Ti 2p peak positions depicted in Fig. 1 are shown in Table 2. Such displacements may suggest changes in the electronic structure of TiO_2 due to the different preparation methods [35,36].

For electrodes prepared through the laser and microwave methods, a shift in the Ti $2p_{3/2}$ peak was observed for lower binding energy values than pure TiO_2, suggesting a charge transfer for the Ti atoms of these anodes [35,36]. Moreover, considering the position of the Ti $2p_{3/2}$ peak o for pure TiO_2 observed by Näslund et al. [33] (Ti $2p_{3/2}$ and Ti $2p_{1/2}$ located at 459.3 and 465.0 eV, respectively), the changes in the electronic structure of TiO_2 observed for the anodes prepared using laser and microwave suggest a strong interaction between Ru and Ti in the films, as will be discussed for the Ru 3d data.

The deconvolution of the high-resolution spectra of Ru 3d + C 1 s is shown in Fig. 2. The Ru $3d_{5/2}$ and Ru $3d_{3/2}$ peaks were deconvoluted into three components for the furnace-prepared anode (Fig. 2c) and fitted into two components for the laser (Fig. 2a) and microwave-prepared (Fig. 2b) anodes.

The lower binding energy of Ru $3d_{5/2}$ at 281.1 eV for the furnace-prepared anode corresponds to the Ru^{4+} oxidation state. The other peaks, at 282 and 283.1 eV, can be assigned to Ru^{6+} and Ru^{8+} oxidation states. The split spin-orbit of 4.7 eV is consistent with the expected Ru^{4+} oxidation state found in RuO_2 species [32–34,37], while the other

Table 2
Peak positions and atomic % for the $Ti/Ru_{0.3}Ti_{0.7}O_2$ anodes.

Heating method	Element	Position (eV)	Atomic %
Furnace	Ru 3d 5/2 I	281.1	7.20
	Ru 3d 5/2 II	282.0	24.93
	Ru 3d 5/2 III	283.1	10.3
	Ru 3d 3/2 I	285.3	1.78
	Ru 3d 3/2 II	286.2	16.46
	Ru 3d 3/2 III	287.3	6.80
	C−C	284.9	16.51
	C−O	286.4	13.62
	C═O	288.3	2.40
	Ti 2p 3/2	459.8	55.78
	Ti 2p 1/2	465.5	27.89
	Ru 3p 3/2 I	463.2	14.46
	Ru 3p 3/2 II	467.4	1.87
Laser	Ru 3d 5/2 I	280.7	29.01
	Ru 3d 5/2 II	282.1	12.16
	Ru 3d 3/2 I	284.5	19.14
	Ru 3d 3/2 II	285.8	8.03
	C−C	284.5	24.28
	C−O	285.7	4.99
	C═O	286.7	2.40
	Ti 2p 3/2	457.9	54.19
	Ti 2p 1/2	463.6	27.10
	Ru 3p 3/2 I	461.4	14.94
	Ru 3p 3/2 II	465.6	3.77
Microwave	Ru 3d 5/2 I	280.8	34.31
	Ru 3d 5/2 II	282.3	10.16
	Ru 3d 3/2 I	284.5	22.65
	Ru 3d 3/2 II	285.9	6.70
	C−C	284.5	24.51
	C−O	286.0	1.04
	C═O	288.8	0.63
	Ti 2p 3/2	458.1	52.26
	Ti 2p 1/2	463.8	26.13
	Ru 3p 3/2 I	461.7	18.58
	Ru 3p 3/2 II	465.9	3.03

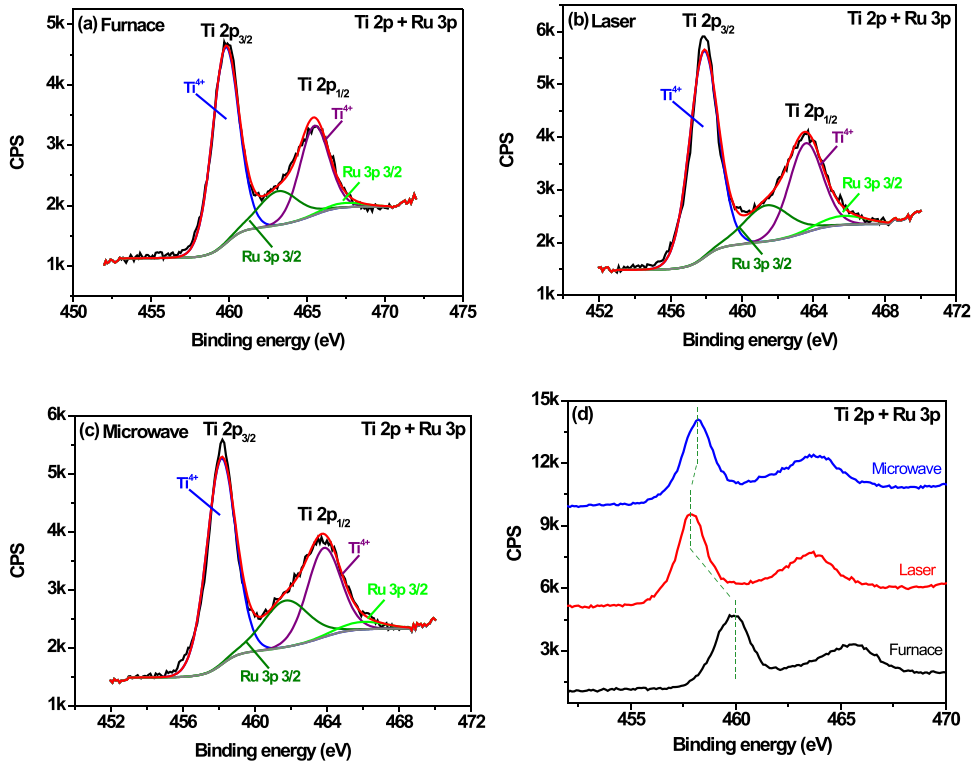

Fig. 1. High-resolution XPS spectra of Ti 2p + Ru $3p_{3/2}$ of the $Ti/Ru_{0.3}Ti_{0.7}O_2$ anodes obtained through the (a) furnace, (b) laser, and (c) microwave methods. (d) Comparison between the Ti 2p spectra of the $Ti/Ru_{0.3}Ti_{0.7}O_2$ anodes. The green dashed lines indicate the shift of the Ti $2p_{3/2}$ peak.

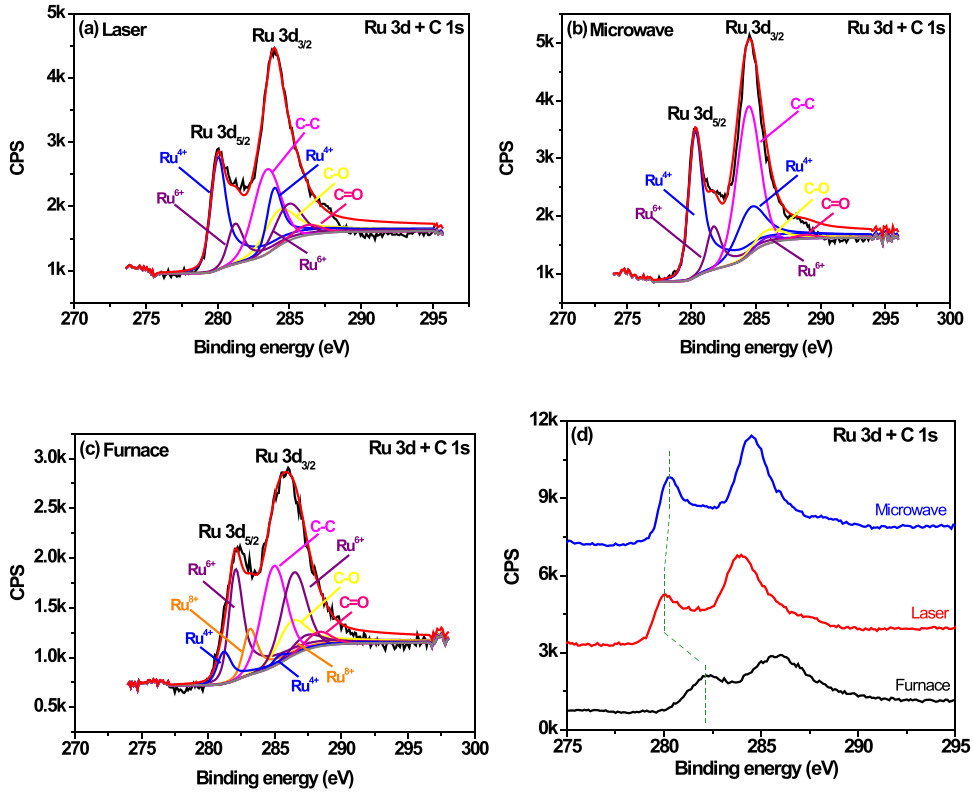

Fig. 2. High-resolution XPS spectra of Ru 3d + C 1 s of the Ti/$Ru_{0.3}Ti_{0.7}O_2$ anodes obtained through the (a) laser, (b) microwave, and (c) conventional methods and (d) comparison between the Ru $3d_{5/2}$ spectra of the Ti/$Ru_{0.3}Ti_{0.7}O_2$ anodes. The green dashed lines indicate the shift of Ru 3d + C 1 s.

oxidation states correspond to RuO_3 and RuO_4 formation.

Two critical differences can be found in the spectra of the Ti/$Ru_{0.3}Ti_{0.7}O_2$ laser- and microwave-made anodes. First, the binding energies of the Ru $3d_{5/2}$ peaks for these materials shifted to lower values, as shown in Fig. 2d and Table 2, which might result from an interfacial reaction between RuO_2 and TiO_2, forming the Ti−O−Ru bond [32]. The second difference is observed in the Ti/$Ru_{0.3}Ti_{0.7}O_2$ furnace-prepared anode spectrum. It is the decrease in the intensities of both RuO_2 peaks, the increase in the intensity of $3d_{5/2}$ RuO_3, and the appearance of RuO_4 contributions. Heating in furnaces takes place from the outside to the inside of the material; consequently, the first layers of the material can be oxidized to form RuO_3. Once the anode surface is completely oxidized, the amount of RuO_3 reaches a certain saturation level, and part of the RuO_3 is oxidized to RuO_4 [30]. Therefore, the ruthenium oxides may form clusters or are in regions of low interaction with Ti atoms at the surface of the anodes made using a furnace.

The peak at 284.6 eV is attributed to graphite's C 1 s binding energy and was used for binding energy calibration. The rest of the components come from the surface C contaminants, C−O and C═O bonds, which are very common surface contaminations on samples exposed to laboratory air [30,38].

The XRD patterns of the RuO_2-TiO_2 powders (after removing them from the substrates) are shown in Fig. 3, alongside the refined patterns obtained by Rietveld analysis. Table SM1 presents the cell parameters and quality factors. The main quality parameter, goodness-of-fit, is less than 1, indicating a good fit between the experimental and refined data. The diffractograms were refined starting from TiO_2 rutile (JCPDS n° 01–076–0320), TiO_2 anatase (JCPDS n° 21–1272), and RuO_2 rutile (JCPDS n° 40–1290) structures. Both TiO_2 and RuO_2 are isostructural with a tetragonal structure and space group P42/mmm. Besides, Ti (0.605 Å – CN = 6) and Ru (0.62 Å – CN = 6) present similar ionic radii facilitating the occupation of the Ru site by Ti and vice versa. Notably, no peak shifts were observed (Fig. SM5). This behavior is also documented in previous studies with RuO_2-TiO_2 because Ru and Ti satisfy the Hume-Rothery conditions for solid solution formation [10, 39]. Thus, for the Rietveld refinement study, two initial strategies were adopted: i) a mixture of the two TiO_2 and RuO_2 phases, in which the data did not converge, and ii) consider Ru (lesser amount) occupying the Ti site in the TiO_2 structure, which was successful. As a consequence, the refinement results suggest the formation of a single compound, or almost completely, with the chemical formula $Ti_{1-x}Ru_xO_2$. The results indicate a Ru occupation factor at about 26% (Table SM1). As expected, the density of the TiO_2-RuO_2 increases, and the cell volume decrease when compared with pure TiO_2. This behavior is due to the Ru (101.07 u) presents a higher atomic mass than Ti (47.867 u) and the cell volume of RuO_2 is more compact than that of TiO_2. These results corroborate the XPS analysis, which suggests a reaction between RuO_2 and TiO_2 to form the Ti−O−Ru bond. Besides, it was detected a small amount (less than 5 mol%) of the TiO_2 Anastasio, whose proportion related to TiO_2-RuO_2 increases in the order of laser < furnace < microwave samples.

Considering the diffractograms in Fig. SM5, in which the XRD measurements were carried out on anodes with the Ti substrate, the curves were normalized in relation to the most intense peak of the Ti substrate. Notably, the relative intensities of the TiO_2-RuO_2 and peaks are more intense for the microwave-made sample, followed by the laser-made and furnace-made anodes, suggesting a better covering for the anode made using microwaves. The difference in relative intensity between the peaks in the diffractograms (Fig. SM5) of the three samples could be related to their crystallinity and crystallite size; that is, the smaller the crystallite size and crystallinity are, the wider and less intense the peaks in the diffractogram. However, the opposite behavior was found; the crystallite sizes (Table 3), which were estimated using the full width at half maximum (FWHM) of the (110) peak and the Scherrer equation, increased for the microwave < laser < furnace samples. Therefore, although the microwave-made anode displays a smaller crystallite size, it has a higher relative intensity than the metallic

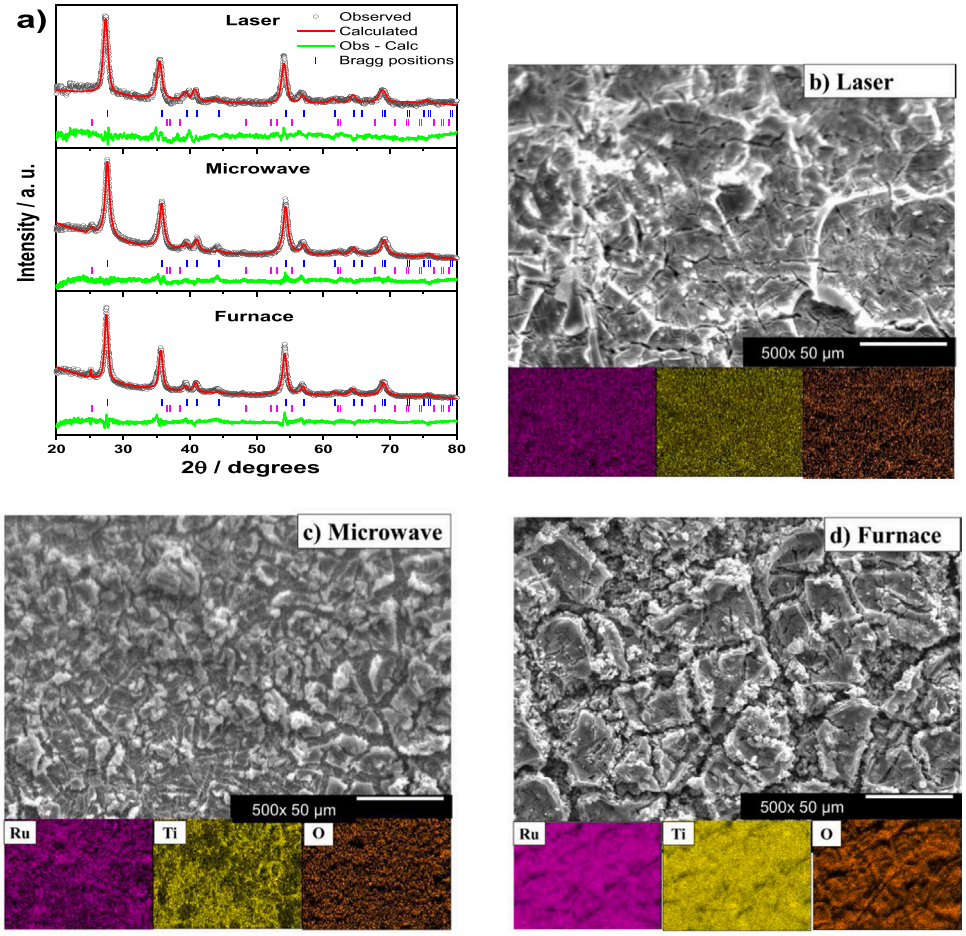

Fig. 3. XRD patterns and Rietveld refinement of the three Ti/RuO_2-TiO_2 studied anodes (a). The black open circles indicate the experimental data, the red line the refined data, the green line the difference between experimental and refined data, and the blue and pink markers are the Bragg positions of the Rutile (JCPDS n° 01–076–0320) and Anatase (JCPDS n° 21–1272) phases, respectively. SEM and EDS mapping images taken for the Ti/RuO_2-TiO_2 anodes synthesized after heat treatments using a laser (b), microwave (c), and furnace (d).

Table 3
The full width at half maximum (FWHM) of the diffraction peak (110), average crystallite size, contact angle, and semiquantitative concentration of the samples under study were determined through the EDS technique.

Heating method	FWHM (for 110)/rad	Crystallite size/nm	Contact angle/°	Composition/mol%	
				Ru	Ti
Laser	0.154	11.5	9.9 ± 5.4	28.04 ± 0.07	71.6 ± 0.13
Microwave	0.205	10.5	26.7 ± 2.5	29.35 ± 0.13	70.65 ± 0.21
Furnace	0.230	12.3	22.8 ± 5.9	28.86 ± 0.07	71.14 ± 0.13

Ti peaks, thus confirming the better coverage of the microwave-produced anodes. The smaller crystallite size has already been reported as a positive contribution to enhancing the active surface area [40].

SEM images obtained with 500 × magnification for the Ti/RuO_2-TiO_2 anodes prepared using microwave (Fig. 3b), furnace (Fig. 3c), and laser (Fig. 3d) heating show rough surfaces for all anodes under study. Likewise, the "mud cracked" texture (a well-known definition for this type of morphology) [17,41] was highly observed on the surface of the furnace-prepared anode with the presence of cracks with greater depth.

SEM images were also used to estimate the pore area at each anode through a thresholding technique based on histogram analysis that segmented the SEM images into pore and nonpore regions. The method used is detailed by Hojat et al. [39]. Fig. SM6 shows the pore size distribution for the anodes prepared by the different heating methods. The electrode prepared by the conventional method (Fig. SM6a) displays a broader pore size distribution, with most of the pores with areas reaching 240 μm^2. The anodes prepared by alternative heating methods showed a narrower pore distribution with smaller pores, mostly 20 μm^2 for the laser (Fig. SM6b) and nearly 70 μm^2 for the anode prepared by microwave heating (Fig. SM6c).

The materials prepared using alternative heating methods (i.e., microwave or laser heating) exhibited this mud-cracked-like morphology but with shallow cracks, indicating that the surfaces are nicely recovered. In particular, the laser-prepared anode presented the most compact surface, which may reflect an improved service life [17,42]. These findings demonstrate that the heating method strongly influences the morphology of the coating. More extended heating periods, as is the case of electrodes prepared in a conventional furnace, lead to a more significant effect of mechanical stress between the substrate and the thin film, increasing the number of cracks in the oxide film surface [8,17]. Thus, the higher the heating time is, the larger the size of the cracks.

EDS analyses of the anodes show that oxide metals were deposited in a proportion very close to nominal, indicating that all heating methods ensure excellent stoichiometric control (Table 3). Moreover, elemental mapping was conducted to investigate the distribution of the metal elements on the surface of the anodes (Fig. 3b-d). The dispersion/distribution of each metal on the Ti/$Ru_{0.3}Ti_{0.7}O_2$ anodes was homogeneous. The contact angle (CA) measurements were conducted to investigate the wettability of the anode's surface. The data in Table 3 show that all anodes have hydrophilic surfaces with CA values ranging from 9.9 ± 5.4–26.7 ± 2.5.

The region between the conduction and valence bands in semiconductor materials is commonly called the bandgap. The literature reports that TiO_2 has a bandgap of approximately 3.2 eV [43]. Therefore, diffuse reflectance spectroscopy measurements (DRS) were

performed to estimate the band gap values of the anodes produced in our study. The heating method does not significantly influence the band gap values of the anodes since the materials synthesized in the microwave, laser, and furnace presented a gap on the order of 3.2 eV (Fig. SM7). The slight decrease in the bandgap observed for the laser- and microwave-prepared electrodes (see Fig. SM7) is probably related to the high interaction between Ru and Ti atoms due to the effects of replacing Ti atoms in the TiO_2 lattice with Ru or the formation of the Ti−O−Ru bond (as mentioned in the XPS discussion) [44].

3.3. Electrochemical characterizations

Fig. 4 shows typical voltammetric profiles for the three anodes at the potential limits of 0.0–1.2 V *vs*. Ag/AgCl. The general analysis of the voltammetric behavior indicates that there is a typical prominent peak of the Ru(III)/Ru(IV) redox transition [45–47] for all anodes. The voltammetric charge recorded in the potential range from 0.0 to 1.2 V (where the OER does not occur) was used to estimate the electrochemically active surface area [48]. The anode prepared using microwave heating has a voltammetric charge of 1.5 and 2.9 times greater than the anodes prepared using laser and furnace heating methods (voltammetric charge values in mC cm^{-2} are shown in Table SM2). Several studies have already reported increasing voltammetric areas for microwave-prepared and laser-prepared anodes. These reports indicate that two factors are responsible for the increase in the voltammetric area. The first is the porous morphology, and the second is the crystallite size reduction presented by anodes prepared using these unconventional methods [8,14,17,18,20].

Another critical feature is the surface and internal active site distribution since the main reactions only occur on the MMO anode surface if it is not permeable. Thus, the morphology factor (φ), calculated according to the methodology developed by Da Silva et al. [28] (Fig. SM8), has been used by several authors to understand better the participation of the external and internal active sites in the total capacitance of anodes [8,14,17]. The higher the value of φ is, the greater the contribution of the inner regions of the oxide layer to the total voltammetric charge, i.e., high values of φ imply that a large portion of the electrochemically active surface area of the MMO is restricted to the inner regions of the oxide coatings, which include surface defects such as narrow pores and cracks [49]. The differential capacitances ($C_{d,t}$, $C_{d,e}$, and $C_{d,i}$, used in the φ calculation) and the φ values related to anodes prepared using different calcination methods are presented in Table SM2. The internal and external differential capacitances vary with the contributions of the internal and external areas. In this way, the high values of the morphology factor presented by anodes prepared by alternative methods (laser 0.81 and microwave 0.94) are associated with the large internal area of the produced anodes, unlike the anode prepared in the furnace, which presented φ of 0.21. Therefore, the anodes made using unconventional heating methods show a high contribution of the internal sites in the total differential capacitance.

EIS is a valuable tool to characterize MMO anodes since it allows the determination of critical electrochemical parameters arising from the reactions occurring at the interface between the electrode and electrolyte [14,19,50]. EIS measurements were performed to study the oxidation of water in H_2SO_4 media. Fig. 4b exhibits the Nyquist plots of the anodes recorded on the OER onset potential. These potential values were selected to ensure the occurrence of water oxidation (determined by linear sweep voltammetry, Fig. SM9). All impedance spectra exhibit only one capacitive loop that is related to the charge transfer process of the OER. The suitable equivalent circuit that best represents the capacitive loop is described as $R_\Omega(R_{ct}Q_{dl})$, where R_Ω is the cell resistance (including connections, electrolyte, and resistance of the oxide deposited), R_{ct} is the charge transfer resistance, and Q_{dl} represents the pseudocapacitance. The use of a constant phase element, CPE, to replace C_{dl} is frequently due to the high degree of roughness and heterogeneity of the electrode surface [17,51].

The fitted EIS data for all three anodes are listed in Table SM2. Notably, the charge transfer resistance calculated for the anode

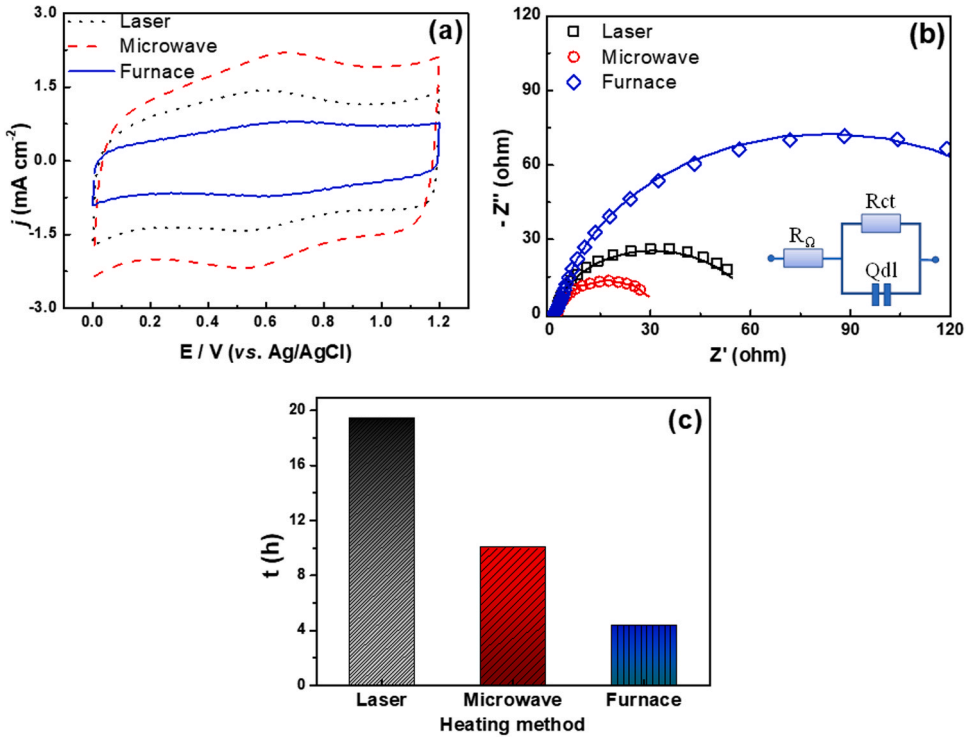

Fig. 4. Cyclic voltammograms obtained at a scan rate of 50 mV s^{-1} (a), Nyquist plots obtained applying an amplitude of 5 mV at the OER onset potential (b), and accelerated service lifetime (ASL) (c) for $Ti/Ru_{0.3}Ti_{0.7}O_2$ anodes obtained after heat treatments using a laser, microwave, or furnace, applying a current density of 500 mA cm^{-2}. All measurements were recorded in 0.5 mol L^{-1} H_2SO_4.

synthesized using microwaves is almost half the R_{ct} value of the laser-prepared anode and 5.6 times lower than the R_{ct} estimated for the anode made using the furnace. The higher R_{ct} value for the furnace-made anode may also be related to higher amounts of RuO_3 and RuO_4 phases, as observed in XPS analysis. In this context, Lisker et al. [52] investigated the effect of annealing on the morphological and electrical properties of iridium and ruthenium thin films in an oxygen atmosphere. They observed a pronounced increase in the ruthenium film resistivity after annealing at 800 °C and concluded that the reduction in the volume of RuO_2 film due to the formation of volatile RuO_3 and RuO_4 phases could explain this increased film resistance. Based on this fact, higher contents of RuO_3 and RuO_4 phases on the anode synthesized using a furnace (data from XPS) may contribute to the higher charge transfer resistance for this anode.

Accelerated service life tests were performed to determine the effect of the heating method on the stability of the anodes (Fig. 4c). Note that the use of laser heating during the coating synthesis improves the service life of the Ti/RuO_2-TiO_2 anode by up to 1.94 and 4.45 times compared with the anodes prepared using a microwave and a furnace. According to Hoseinieh and Ashrafizadeh [53], the deactivation of electrodes containing ruthenium and titanium oxides can be attributed to the dissolution of the components of the oxide layer or the formation of nonconductive layers. The electrode deactivation process is mainly influenced by the electrode composition and the conditions employed in the synthesis [11,18,47]. The penetration of water through the coating into the substrate would affect the stability/passivation of the coated anode. Hence, the morphology of the coating through a porous or cracked structure would affect the water penetration rate. A layer with more cracks, such as the anode calcined in the furnace (as seen in the SEM images of Fig. 3d), appears to be more accessible to water penetration and, therefore, easier to passivate. On the other hand, anodes with more compact morphologies, such as those prepared by microwave and laser heating, showed greater stability. Additionally, deeper cracks can facilitate water permeation to reach the substrate, negatively affecting the anode stability.

3.4. Electrocatalytic efficiency in hypochlorite generation and ciprofloxacin degradation

In electrochemical systems operating in chloride media, chloride ions in the electrolyte solution can be converted directly into active chlorine species (Eq. 3). Other disproportionate chlorine species, such as HClO species and Cl^-, as indicated in Eq. (4), can also participate. As the pKa value of HClO is 7.5, it establishes equilibrium with ClO^- species and the contaminants are oxidized by ClO^- species in solution pH > 7.5, as represented in Eqs. (5), (6) [54].

$$2Cl^- \rightarrow Cl_2 + 2e^- (E^\circ = 1.36\ V/SHE) \quad (3)$$

$$Cl_2 + H_2O \rightarrow HClO + Cl^- + H^+ (E^\circ = 1.49\ V/SHE) \quad (4)$$

$$HClO \rightleftharpoons ClO^- + H^+ (E^\circ = 0.89\ V/SHE) \quad (5)$$

$$ClO^- + C_{17}H_{18}FN_3O_3 \rightarrow \text{intermediates} \quad (6)$$

Thus, under the conditions studied here (initial pH of approximately 6), the formation of hypochlorite and hypochlorous acid is expected, and their efficiency in treating a wide variety of effluents has already been reported [42,55,56]. Fig. 5 shows the concentration of the active chlorine (measured as ClO^-) during electrolysis (Fig. 5a) and electrolysis photoassisted (Fig. 5b) using the anodes prepared by different heating methods as a function of electrolysis time. The hypochlorite concentration increased as a function of time for all anodes. However, when UVC light irradiated the solution, the hypochlorite concentration was much lower than that for the electrolysis process. This fact indicates that chlorine and hydroxyl radicals can be formed by a homolytic reaction of HClO by UVC radiation in the bulk solution (Eq. 6) [54,57].

$$HClO + h\upsilon \rightarrow Cl^- + OH^\bullet \quad (7)$$

These radicals are expected to improve the oxidation and mineralization of pollutants in the electrochemical photoassisted process compared with single electrochemical oxidation or photolysis only since the standard potential values of these species are higher than that of Cl_2, HOCl, ClO^- [58,59].

In electrolysis, the laser-prepared anode was the most efficient for hypochlorite electrochemical generation compared to microwave and furnace anodes (laser > microwave > furnace). In the photoassisted electrolysis, the laser-prepared anode showed the lowest hypochlorite concentration after one hour, followed by the microwave-prepared anode and the furnace-prepared anode in sequence. This fact reinforces the conjecture that the anode with the highest efficiency for the electrogeneration of hypochlorite also has greater catalytic efficiency in generating other chlorine species. In this context, as previously reported for the photoassisted electrolysis occurring in chlorine media, the formation of $Cl^\bullet$ and $OH^\bullet$ is expected [59]. Also, in chlorine media, the formation of stable end-products such as ClO_3^- and ClO_4^- must not be excluded. None ClO_4^- species were detected after 1 h of photoelectrolysis; however, ClO_3^- species were accumulated in quite close concentrations for all anodes (~75 mg L^{-1}). Likewise, ClO_4^- was not detected for electrolysis, while ClO_3^- was detected in negligible concentrations. It is an expected result, as $OH^\bullet$ radicals are not formed in appreciable amounts on the surface of mixed metal oxide anodes during electrolysis. Similar behavior was already reported in the literature [55,59]. For example, Sánchez-Montes et al. [61] studied the removal of the herbicide glyphosate by the electrochemical oxidation process under UVC irradiation in the presence of NaCl and using a dimensionally stable anode. In this study, the authors reported the presence of undesired ClO_3^- species at high concentrations, possibly formed by consecutive HClO hydroxylation reactions on the anode surface and within the solution when UVC light is irradiated [61]. The removal of both

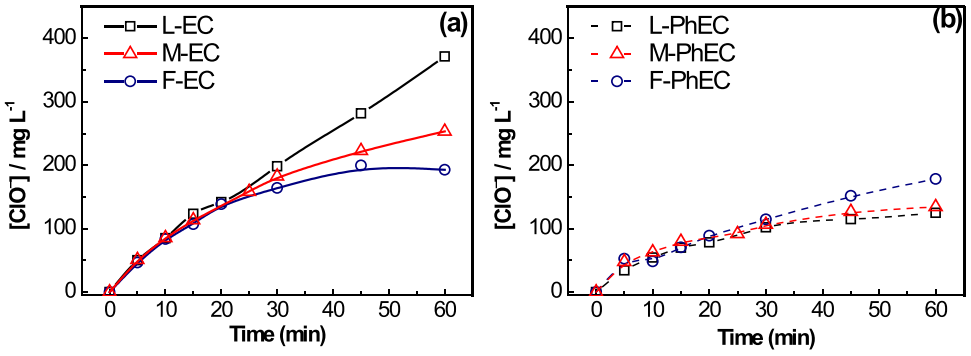

Fig. 5. Evolution of ClO^- concentration as a function of time during electrolysis (EC) (a) and electrolysis photoassisted (PhEC) (b) for Ti/RuO_2-TiO_2 anodes obtained after heat treatments using a laser (L), microwave (M), or furnace (F). All measurements were performed in 3.7 g L^{-1} NaCl, j = 30 mA cm^{-2}, and P_{lamp} = 9 W.

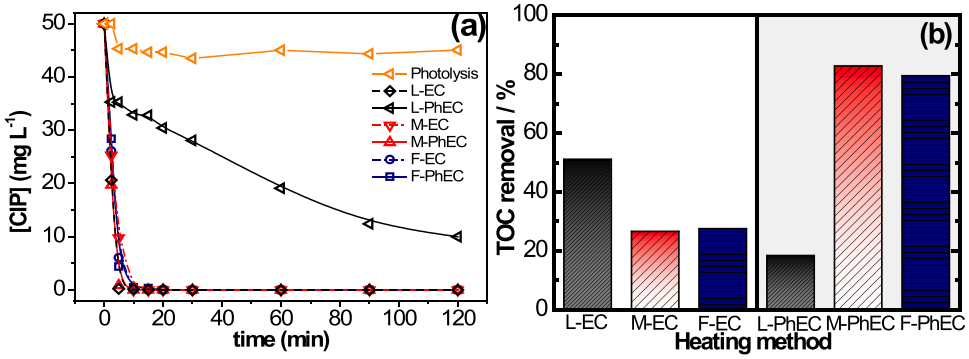

Fig. 6. Decay of CIP concentration as a function of time (a) and TOC removal (b) in photolysis, electrolysis (EC), and electrolysis photoassisted (PhEC) processes using Ti/RuO_2-TiO_2 anodes obtained after heat treatments using a laser, microwave, or furnace. All measurements were performed in 3.7 g L^{-1} NaCl, j = 30 mA cm^{-2}, and P_{lamp} = 9 W.

ciprofloxacin and TOC during irradiated and nonirradiated electrochemical processes for the different synthesized anodes are shown in Fig. 6.

In two hours of treatment, photolysis alone did not significantly remove the contaminant (~10%) and did not remove TOC (information not shown in the figure). Fig. 6a shows the decay of CIP concentration as a function of time. The EC process can completely remove the compound in the first 15 min for all prepared anodes. For this process, TOC removal for EC using the laser-prepared anode (Fig. 6b) was 24% higher than that for the microwave and furnace-prepared anodes (both with approximately 27% TOC removal after 2 h). This result is likely related to the higher production of active chlorine species, as shown in Fig. 5a.

The UVC light coupled with the EC process increased the kinetics of CIP removal by 2.2 and 1.76 times when using the anodes prepared in the microwave and furnace, respectively (Fig. SM10 and Table 4). Additionally, the TOC removal increased approximately 3-fold compared with the EC process alone. Unexpectedly, the effect of UVC light on electrolysis using the laser-prepared anode did not favor the removal of the compound. Consequently, the removal of TOC was decreased compared with electrolysis. At this point, it is important to note that negligible influence of light on the electrode is expected in these electrodes since, as previously shown, the percentage of the photoactive anatase phase of TiO_2 (calculated by XRD analysis) in the anodes is too small to produce photoactivity. Despite that, qualitative photocurrent analyses were carried out in which linear voltammetry experiments were recorded in the presence of UVC 9 W light and dark conditions. As expected, the linear voltammetry curves remained unchanged after illumination, confirming that no additional species were formed on the surface of the anodes during illumination.

In order to explain this unexpected antagonistic behavior, excessive formation of radicals may occur in the application of electrochemical technologies assisted by coupled UVC irradiation and must be considered. Instead of attacking organic species, the $^{\bullet}OH$ and $Cl^{\bullet}$ radicals can suffer self-recombination to form more stable and less aggressive species [60]. Moreover, from further analysis of chromatograms extracted from HPLC, it is possible to clarify that aromatic by-products (additional peaks that appear and decrease with time) generated during the electrochemical photoassisted process using laser-prepared anodes are the same as during the same process using the other two anodes (micro- and furnace-prepared) (Fig. SM11). This observation strongly suggests that the changes in kinetic rates observed in Fig. 6 and Table 4 are only associated with the efficiency of the oxidants produced and do not depend on the reaction mechanism.

Regarding the mechanisms of the electrochemical and photoassisted electrochemical oxidation processes using the Ti/RuO_2-TiO_2 anodes prepared in the present study, the degradation of organics from water occurs by the action of strong oxidation species, including Cl_2, HClO, $^{\bullet}Cl$, and $^{\bullet}OH$, as previously discussed here. Subsequently, these species can quickly oxidize ciprofloxacin leading to partial mineralization (inorganics ions, CO_2, and H_2O), as depicted in Fig. 7.

According to the mechanism of electrochemical oxidation, direct and indirect routes takes place. In the direct route, ciprofloxacin diffuses to the anode surface, where it is oxidized by chemisorbed ($^{\bullet}OH$). In the presence of chlorine, an indirect route occurs by the action of active chlorine (mainly HClO/ClO^-) at pH 6, formed via the chlorine evolution reaction. Similarly, photoassisted electrochemical oxidation with Ti/RuO_2-TiO_2 anode also presents direct and indirect routes. However, the enhanced performance of photoassisted electrochemical oxidation is mainly explained by the formation of stronger oxidants (mainly $^{\bullet}Cl$ and $^{\bullet}OH$) by photo-excitation using UVC irradiation (254 nm).

Electrochemical technologies to treat pollutants must consider energy consumption to enable their implementation. Thus, the efficiency of this process was evaluated through the consumption of electricity per TOC removed (Table 5). In the nonirradiated electrochemical oxidation processes, and depending on the synthesis method of the anode, the increase in energy consumption followed the order laser < microwave < furnace. This sequence is related to the increased electron transfer resistance displayed by the furnace-made anodes, as shown in the EIS measurements (Fig. 4b). Likewise, the use of UVC irradiation promotes a significant increase in energy consumption due to the presence of the lamp. The highest energy consumption was observed for the PhEC laser process due to the lower TOC removal obtained under this condition.

Comparing CIP electrochemical oxidation results obtained in our study with the available literature is challenging since different conditions are used (pH, electrolyte, current density, anode composition, and volumetric flow, among others). Table 5 compares CIP removal outcomes obtained using electrodes with different compositions regarding the compound and TOC removal kinetic rate under the best operating conditions obtained in each study. For example, Antonelli et al. [4] studied the removal of CIP by electrochemical oxidation using a commercial Ti/$Ru_{0.3}Ti_{0.7}O_2$ anode in a NaCl medium. The compound removal rate and TOC removal (0.8 min^{-1} and 60%) outcomes using the PhEC process are close to those found in our work using PhEC with the electrode prepared through microwave heating (0.73 min^{-1} and 82.8%). Likewise, the compound removal rate (0.74 min^{-1}) and TOC removal

Table 4
Kinetic constants and EEO values for CIP removal by the different processes.

Heating method	Process	k/min^{-1}	R^2	EC_{TOC}/kWh g^{-1}TOC
	Photolysis	0.006	0.57	–
Laser	EC	0.53	0.89	0.43
	PhEC	0.03	0.76	32.18
Microwave	EC	0.33	0.91	0.82
	PhEC	0.73	0.99	7.14
Furnace	EC	0.37	0.93	1.16
	PhEC	0.65	0.96	7.45

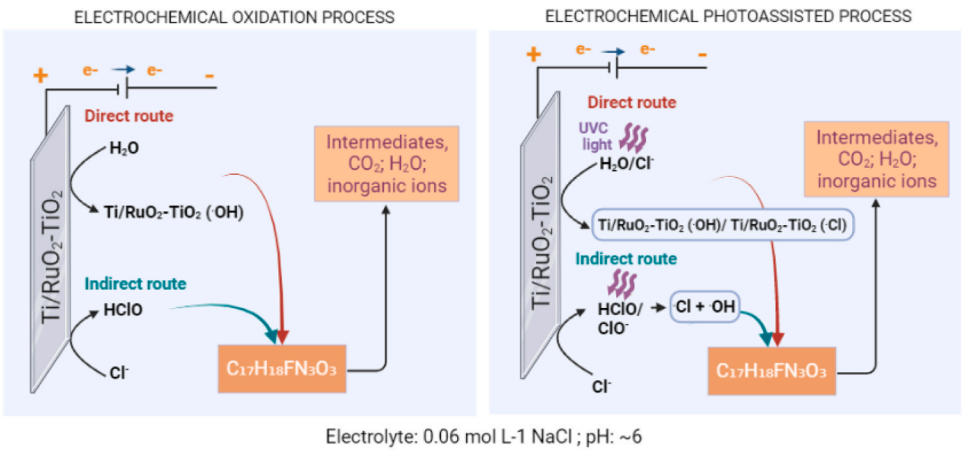

Fig. 7. Schematic diagrams of direct and indirect degradation mechanism on Ti/RuO_2-TiO_2 anode surface under electrochemical (a) and electrochemical photo-assisted process.

Table 5
Comparison of the performances of different anodes for the oxidation of ciprofloxacin in NaCl medium.

Anode	Experimental conditions	k (min^{-1})	TOC removal	Reference
Ti/$Ru_{0.3}Ti_{0.7}O_2$ (De Nora®) (15 cm^2)	j = 60.7 mA cm^{-2}, [CIP] = 368 mg L^{-1}, [NaCl] = 0.3 mol L^{-1}, V = 0.2 L, t = 60 min	0.74 (EC) 0.8 (PhEC)	56% (EC) 60% (PhEC)	[4]
Ti/SnO_2-Sb (4 cm^2)	j = 20 mA cm^{-2}, [CIP] = 30 mg L^{-1}, [Na_2SO_4] = 25 g L^{-1}, V = 0.05 L, t = 60 min	0.0506	–	[62]
Boron-doped diamond (10 cm^2)	j = 30 mA cm^{-2}, [CIP] = 10 mg L^{-1}, [Na_2SO_4]= 0.05 mol L^{-1}, V= 0.3 L, t = 120 min	0.10	50% DOC*	[63]
Ti/SnO_2-Sb (15 cm^2)	j = 30 mA cm^{-2}, [CIP] = 50 mg L^{-1}, [Na_2SO_4] = 0.5 mol L^{-1}, V = 0.25 L, t = 120 min	0.046	70%	[64]
Sb_2O_5 doped-Ti/RuO_2-ZrO_2 (4 cm^2)	j = 17 mA cm^{-2}, [CIP] = 50 mg L^{-1}, [NaCl] = 0.5 mol L^{-1}, V = 0.13 L	–	40%	[65]
Laser-made Ti/RuO_2-TiO_2 (2 cm^2)	j = 30 mA cm^{-2}; [CIP] = 50 mg L^{-1}; [NaCl] = 3.7 g L^{-1}, V = 0.1 L, t = 120 min	0.53 (EC)	51.1%	This work
Microwave-made Ti/RuO_2-TiO_2 (2 cm^2)	j = 30 mA cm^{-2}; [CIP] = 50 mg L^{-1}; [NaCl]= 3.7 g L^{-1}, V = 0.1 L, t = 120 min	0.73 (PhEC)	82.8%	This work

* dissolved organic carbon (DOC).

(56%) using the EC process were slightly higher than the outcomes obtained here using the laser-made anode (0.53 min^{-1} and 51.1%). However, it is worth mentioning the huge discrepancy in the initial CIP concentration values (368 mg L^{-1} versus 50 mg L^{-1}) and the anode area/volume of the treated solution (15 cm^2/200 mL versus 2 cm^2/100 mL) in that report compared with our work.

Moreover, Li et al. [63] and Wang et al. [64] studied the optimal current density for the electrochemical removal of CIP using boron-doped diamond (BDD) and Ti/SnO_2-Sb anodes. Among the current densities studied (10–40 mA cm^{-2}) by Li et al. [63], 30 mA cm^{-2} was the most advantageous, as a reduction of at least 15% of the electrical efficiency value per order was obtained. Wang et al. [64] also showed that among the current density range used, 10–40 mA cm^{-2}, the application of 30 mA cm^{-2} yielded the highest removal rate of CIP (0.046 min^{-1}), TOC (70.0%) and COD (86.0%). Remarkably, the CIP removal rates taken using the nonactive anodes BDD [63] (0.10 min^{-1}), Ti/SnO_2-Sb [64] (0.046 min^{-1}), and Ti/SnO_2-Sb [62] (0.0506 min^{-1}) are 5.3-, 10.5-, and 11.5-fold lower than the removal rate seen using the active Ti/RuO_2-TiO_2 anode produced using laser heating (0.53 min^{-1}). Note that the active Ti/RuO_2-TiO_2 anode made using microwave heating also displays a higher CIP removal rate (0.33 min^{-1}) than the nonactive anodes BDD and Ti/SnO_2-Sb under the best operating conditions of each study.

In general, the expansion potential of electrochemical processes in environmental electrochemistry is undoubtedly promising. The significant progress in the development of new anodes points to the improvement of these processes. Consequently, they might demonstrate the relevance of electrochemistry as a plausible and reliable alternative.

4. Conclusions

This study demonstrates the synthesis, characterization, and effective application of Ti/RuO_2-TiO_2 anodes synthesized by innovative CO_2 laser and microwave heating. The extensive characterization and catalytic evaluation of the anodes revealed several essential aspects, which are summarized below.

- Physical characterizations indicated the presence of RuO_2 and TiO_2 formed as a metastable solid solution for all anodes. Additionally, the alternative heating methods studied led to more compact surfaces associated with lower heating and cooling periods for these methods. These changes in the morphology of the surfaces are reflected in the improved service life of these anodes.
- The anode made using microwaves showed the largest voltammetric area (83.31 mC cm^{-2}) and lowest charge transfer resistance (29.75 Ω). However, the highest stability was presented by the anode prepared by the laser (approximately 20 h of durability under severe conditions), according to the results from the surface analysis.
- Electrolysis carried out in NaCl media generated a large amount of active chlorine, unquestionably the primary source of indirect oxidation. Using the laser-prepared anodes in electrolysis, the generation of ClO^- was the highest (372 mg L^{-1} ClO^-), and the mineralization of ciprofloxacin (51%) was the greatest among the anodes studied. Unexpectedly, the laser-prepared anode in the photoassisted electrochemical process presented the worst performance in pollutant removal and mineralization, probably due to parasitic propagation reactions involving ClO^- species. Thus, this anode under these conditions should be avoided.

- Finally, the photoassisted electrochemical process using the microwave-prepared anode appears to be the best option for removing ciprofloxacin in chloride media, leading to the best outcome regarding energy consumption per TOC removed.

CRediT authorship contribution statement

Aline R. Dória: Methodology, Investigation, Validation, Writing – original draft. **Isabelle M. D. Gonzaga:** Methodology, Investigation, Validation, Writing – original draft. **Gessica de O. S. Santos**: Visualization, Investigation, Writing - Original Draft. **Caio V.S. Almeida:** Methodology, Investigation, Writing – original draft. **Deyvid C. Silva:** Methodology, Investigation. **Ronaldo S. Silva:** Funding acquisition, Conceptualization, Writing – review & editing. **Luciane P. C. Romão:** Visualization, Conceptualization, Writing – review & editing. **Cristina Sáez:** conceptualization, Writing – review & editing. **Giancarlo R. Salazar-Banda:** Supervision, Funding acquisition, Conceptualization, Writing – review & editing. **Katlin I. B. Eguiluz:** Supervision, Funding acquisition, Conceptualization, Writing – review & editing.

Declaration of Competing Interest

The authors declare that they have no known competing financial interests or personal relationships that could have appeared to influence the work reported in this paper.

Data Availability

Data will be made available on request.

Acknowledgments

This study was also financed by the Brazilian agencies Coordenaç ão de Aperfeiçoamento de Pessoal de N í vel Superior - CAPES (88887.157964/2017–00), CNPq (142034/2020–7, 305438/2018–2, and 311856/2019–5) and FAPITEC/SE. Financial support from Ministry of Science and Innovation of Spain through the project PID 2019-110904RB-I00 is also acknowledged. The authors thank the Center for Study on Colloidal Systems (NUESC) for the diffuse reflectance spectroscopy analyses.

Appendix A. Supporting information

Supplementary data associated with this article can be found in the online version at doi:10.1016/j.apcatb.2023.123092.

References

[1] S.W. da Silva, J.B. Welter, L.L. Albornoz, A.N.A. Heberle, J.Z. Ferreira, A. M. Bernardes, Advanced oxidation processes the treatment of pharmaceutical containing water and wastewater: a review, Curr. Pollut. Rep. 7 (2021) 146–159, https://doi.org/10.1007/s40726-021-00176-6.

[2] W.T. Jiang, P.H. Chang, Y.S. Wang, Y. Tsai, J.S. Jean, Z. Li, K. Krukowski, Removal of ciprofloxacin from water by birnessite, J. Hazard. Mater. 250–251 (2013) 362–369, https://doi.org/10.1016/j.jhazmat.2013.02.015.

[3] S. Rakshit, D. Sarkar, E.J. Elzinga, P. Punamiya, R. Datta, Mechanisms of ciprofloxacin removal by nano-sized magnetite, J. Hazard. Mater. 246–247 (2013) 221–226, https://doi.org/10.1016/j.jhazmat.2012.12.032.

[4] R. Antonelli, G.R.P. Malpass, M.G.C. da Silva, M.G.A. Vieira, Photo-assisted electrochemical degradation of ciprofloxacin using DSA® anode with NaCl electrolyte and simultaneous chlorine photolysis, J. Water Process Eng. 47 (2022), 102698, https://doi.org/10.1016/j.jwpe.2022.102698.

[5] I. Sirés, E. Brillas, M.A. Oturan, M.A. Rodrigo, M. Panizza, Electrochemical advanced oxidation processes: today and tomorrow. A review, Environ. Sci. Pollut. Res. 21 (2014) 8336–8367, https://doi.org/10.1007/s11356-014-2783-1.

[6] M.C. Vagi, A.S. Petsas, Recent advances on the removal of priority organochlorine and organophosphorus biorecalcitrant pesticides defied by Directive 2013/39/EU from environmental matrices by using advanced oxidation processes: an overview (2007-2018), J. Environ. Chem. Eng. (2019), 102940, https://doi.org/10.1016/j.jece.2019.102940.

[7] G.R. Salazar-Banda, G. de, O.S. Santos, I.M. Duarte Gonzaga, A.R. Dória, K.I. Barrios Eguiluz, Developments in electrode materials for wastewater treatment, Curr. Opin. Electrochem 26 (2021), 100663, https://doi.org/10.1016/j.coelec.2020.100663.

[8] A.R. Dória, G.O.S. Santos, M.M.S. Pelegrinelli, D.C. Silva, D.B. de Matos, E. B. Cavalcanti, R.S. Silva, G.R. Salazar-Banda, K.I.B. Eguiluz, Improved 4-nitrophenol removal at Ti/RuO_2–Sb_2O_4–TiO_2 laser-made anodes, Environ. Sci. Pollut. Res. 28 (2021) 23634–23646, https://doi.org/10.1007/s11356-020-10451-6.

[9] W. Wu, Z.-H. Huang, T.-T. Lim, Recent development of mixed metal oxide anodes for electrochemical oxidation of organic pollutants in water, Appl. Catal. A Gen. 480 (2014) 58–78, https://doi.org/10.1016/j.apcata.2014.04.035.

[10] A.R. Dória, I.M.D. Gonzaga, G.O.S. Santos, M. Pupo, D.C. Silva, R.S. Silva, M. A. Rodrigo, K.I.B. Eguiluz, G.R. Salazar-Banda, Ultra-fast synthesis of Ti/$Ru_{0.3}Ti_{0.7}O_2$ anodes with superior electrochemical properties using an ionic liquid and laser calcination, Chem. Eng. J. 416 (2021), 129011, https://doi.org/10.1016/j.cej.2021.129011.

[11] C.W. dos A. Bezerra, G. de O.S. Santos, M.M. de S. Pupo, M. de A. Gomes, R.S. da Silva, K.I.B. Eguiluz, G.R. Salazar-Banda, Novel eco-friendly method to prepare Ti/RuO_2–IrO_2 anodes by using polyvinyl alcohol as the solvent, J. Electroanal. Chem. 859 (2020), 113822, https://doi.org/10.1016/j.jelechem.2020.113822.

[12] F. Moradi, C. Dehghanian, Influence of heat treatment temperature on the electrochemical properties and corrosion behavior of RuO_2-TiO_2 coating in acidic chloride solution, Prot. Met. Phys. Chem. Surf. 49 (2013) 699–704, https://doi.org/10.1134/S2070205113060245.

[13] V. Krstić, B. Pešovski, Reviews the research on some dimensionally stable anodes (DSA) based on titanium, Hydrometallurgy 185 (2019) 71–75, https://doi.org/10.1016/j.hydromet.2019.01.018.

[14] I.M.D. Gonzaga, A.R. Dória, V.M. Vasconcelos, F.M. Souza, M.C. dos Santos, P. Hammer, M.A. Rodrigo, K.I.B. Eguiluz, G.R. Salazar-Banda, Microwave synthesis of Ti/$(RuO_2)_{0.5}(IrO_2)_{0.5}$ anodes: improved electrochemical properties and stability, J. Electroanal. Chem. 874 (2020), 114460, https://doi.org/10.1016/j.jelechem.2020.114460.

[15] M.O. Santos, G. de, O.S. Santos, S. Mattedi, S. Griza, K.I.B. Eguiluz, G.R. Salazar-Banda, Influence of the calcination temperature and ionic liquid used during synthesis procedure on the physical and electrochemical properties of Ti/$(RuO_2)_{0.8}$–$(Sb_2O_4)_{0.2}$ anodes, J. Electroanal. Chem. 829 (2018) 116–128, https://doi.org/10.1016/j.jelechem.2018.10.013.

[16] M.N.G. dos Reis, A.S. Ramos Neto, V.M. Vasconcelos, A.R. Dória, G.O.S. Santos, E. A. dos Santos, K.I.B. Eguiluz, G.R. Salazar-Banda, Ti/$Ru_{0.7}M_{0.3}O_2$ (M = Ir or Ti) anodes made by Pechini and ionic liquid methods: Uneven catalytic activity and stability, J. Electroanal. Chem. 895 (2021), 115461, https://doi.org/10.1016/j.jelechem.2021.115461.

[17] G.O.S. Santos, L.R.A. Silva, Y.G.S. Alves, R.S. Silva, K.I.B. Eguiluz, Enhanced stability and electrocatalytic properties of Ti/$Ru_xIr_{1-x}O_2$ anodes produced by a new laser process, Chem. Eng. J. (2018), https://doi.org/10.1016/j.cej.2018.08.145.

[18] V.M. Vasconcelos, I.M.D. Gonzaga, A.R. Dória, P.J.M. Cordeiro-Junior, M.R. V. Lanza, K.I.B. Eguiluz, G.R. Salazar-Banda, Effects of temperature and heating method on the performance of Ti/$Ru_{0.25}Ir_{0.25}Ti_{0.50}O_2$ anodes applied toward Bisphenol S removal, Electrochim. Acta 364 (2020), 137273, https://doi.org/10.1016/j.electacta.2020.137273.

[19] A.R. Dória, R.S. Silva, P.H. Oliveira Júnior, E.A. dos Santos, S. Mattedi, P. Hammer, G.R. Salazar-Banda, K.I.B. Eguiluz, Influence of the RuO_2 layer thickness on the physical and electrochemical properties of anodes synthesized by the ionic liquid method, Electrochim. Acta 354 (2020), https://doi.org/10.1016/j.electacta.2020.136625.

[20] G.O.S. Santos, A.R. Dória, V.M. Vasconcelos, C. Sáez, M.A. Rodrigo, K.I.B. Eguiluz, G.R. Salazar-Banda, Enhancement of wastewater treatment using novel laser-made Ti/SnO_2–Sb anodes with improved electrocatalytic properties, Chemosphere 259 (2020), 127475, https://doi.org/10.1016/j.chemosphere.2020.127475.

[21] S.S. Lephuthing, A.M. Okoro, O.O. Ige, P.A. Olunambi, Microstructural and electrochemical studies of spark plasma sintered multiwall carbon nanotubes reinforced TiO_2-MnO_2 based composite, J. Mater. Res. Technol. 12 (2021) 894–903, https://doi.org/10.1016/j.jmrt.2021.03.003.

[22] M.T. Colomer, J.R. Jurado, Structural, microstructural, and electrical transport properties of TiO_2-RuO_2 ceramic materials obtained by polymeric sol-gel route, Chem. Mater. 12 (2000) 923–930, https://doi.org/10.1021/cm9903879.

[23] J.D. García-Espinoza, I. Robles, A. Durán-Moreno, L.A. Godínez, Photo-assisted electrochemical advanced oxidation processes for the disinfection of aqueous solutions: a review, Chemosphere 274 (2021), https://doi.org/10.1016/j.chemosphere.2021.129957.

[24] M.T. Uddin, O. Babot, L. Thomas, C. Olivier, M. Redaelli, M. D'Arienzo, F. Morazzoni, W. Jaegermann, N. Rockstroh, H. Junge, T. Toupance, New insights into the photocatalytic properties of RuO_2/TiO_2 mesoporous heterostructures for hydrogen production and organic pollutant photodecomposition, J. Phys. Chem. C. 119 (2015) 7006–7015, https://doi.org/10.1021/jp512769u.

[25] M.T. Uddin, Y. Nicolas, C. Olivier, T. Toupance, M.M. Müller, H.J. Kleebe, K. Rachut, J. Ziegler, A. Klein, W. Jaegermann, Preparation of RuO_2/TiO_2 mesoporous heterostructures and rationalization of their enhanced photocatalytic properties by band alignment investigations, J. Phys. Chem. C. 117 (2013) 22098–22110, https://doi.org/10.1021/jp407539c.

[26] P. García-Ramírez, E. Ramírez-Morales, J.C. Solis Cortazar, I. Sirés, S. Silva-Martínez, Influence of ruthenium doping on UV- and visible-light photoelectrocatalytic color removal from dye solutions using a TiO_2 nanotube array photoanode, Chemosphere 267 (2021), https://doi.org/10.1016/j.chemosphere.2020.128925.

[27] R. de Mello, L.H.E. Santos, M.M.S. Pupo, K.I.B. Eguiluz, G.R. Salazar-Banda, A. J. Motheo, Alachlor removal performance of Ti/$Ru_{0.3}Ti_{0.7}O_2$ anodes prepared from ionic liquid solution, J. Solid State Electrochem 22 (2018) 1571–1580, https://doi.org/10.1007/s10008-017-3700-6.

[28] L. Da Silva, L. De Faria, J.F. Boodts, Determination of the morphology factor of oxide layers, Electrochim. Acta 47 (2001) 395–403, https://doi.org/10.1016/S0013-4686(01)00738-1.

[29] Y. Liu, H. Liu, J. Ma, J. Li, Preparation and electrochemical properties of Ce-Ru-SnO_2 ternary oxide anode and electrochemical oxidation of nitrophenols, J. Hazard. Mater. 213– 214 (2012) 222–229, https://doi.org/10.1016/j.jhazmat.2012.01.090.

[30] B. Hudec, K. Hušeková, A. Rosová, J. Šoltýs, R. Rammula, A. Kasikov, T. Uustare, M. Mičušík, M. Omastová, J. Aarik, K. Fröhlich, Impact of plasma treatment on electrical properties of TiO_2/RuO_2 based DRAM capacitor, J. Phys. D. Appl. Phys. 46 (2013), https://doi.org/10.1088/0022-3727/46/38/385304.

[31] W. Wang, S. Guo, I. Lee, K. Ahmed, J. Zhong, Z. Favors, F. Zaera, M. Ozkan, C. S. Ozkan, Hydrous ruthenium oxide nanoparticles anchored to graphene and carbon nanotube hybrid foam for supercapacitors, Sci. Rep. 4 (2014) 9–14, https://doi.org/10.1038/srep04452.

[32] M.T. Uddin, Y. Nicolas, C. Olivier, T. Toupance, M.M. Müller, H.J. Kleebe, K. Rachut, J. Ziegler, A. Klein, W. Jaegermann, Preparation of RuO_2/TiO_2 mesoporous heterostructures and rationalization of their enhanced photocatalytic properties by band alignment investigations, J. Phys. Chem. C. 117 (2013) 22098–22110, https://doi.org/10.1021/jp407539c.

[33] L.Å. Näslund, C.M. Sánchez-Sánchez, Á.S. Ingason, J. Bäckström, E. Herrero, J. Rosen, S. Holmin, The role of TiO_2 doping on RuO_2-coated electrodes for the water oxidation reaction, J. Phys. Chem. C. 117 (2013) 6126–6135, https://doi.org/10.1021/jp308941g.

[34] H. Yue, L. Xue, F. Chen, Efficiently electrochemical removal of nitrite contamination with stable RuO_2-TiO_2/Ti electrodes, Appl. Catal. B Environ. 206 (2017) 683–691, https://doi.org/10.1016/j.apcatb.2017.02.005.

[35] I. Takahashi, D.J. Payne, R.G. Palgrave, R.G. Egdell, High resolution X-ray photoemission study of nitrogen doped TiO_2 rutile single crystals, Chem. Phys. Lett. 454 (2008) 314–317, https://doi.org/10.1016/j.cplett.2008.02.031.

[36] M. Sathish, B. Viswanathan, R.P. Viswanath, C.S. Gopinath, Synthesis, Characterization, Electronic Structure, and Photocatalytic Activity of Nitrogen-Doped TiO2 Nanocatalyst, (2005) 6349–6353.

[37] A.V. Naumkin, A. Kraut-Vass, S.W. Gaarenstroom, C.J. Powell, X-ray photoelectron spectroscopy database, Standard Reference Database 20, Htttp. Srdata. Nist. Gov/XPS. 4.1 (n.d.).

[38] O.L. Hendricks, A.G. Scheuermann, M. Schmidt, P.K. Hurley, P.C. McIntyre, C.E. D. Chidsey, Isolating the photovoltaic junction: atomic layer deposited TiO_2-RuO_2 alloy schottky contacts for silicon photoanodes, ACS Appl. Mater. Interfaces 8 (2016) 23763–23773, https://doi.org/10.1021/acsami.6b08558.

[39] W.A. Gerrard, B.C.H. Steele, Microstructural investigations on mixed RuO_2-TiO_2 coatings, J. Appl. Electrochem 8 (1978) 417–425, https://doi.org/10.1007/BF00615837.

[40] Y. Xin, L. Xu, J. Wang, The deactivation mechanism of RuO_2-IrO_2-SnO_2/Ti anodes under alternative current electrolysis condition, Proc. 2015 3rd Int. Conf. Mach. Mater. Inf. Technol. Appl. 35 (2015) 1762–1765, https://doi.org/10.2991/icmmita-15.2015.328.

[41] L.M. da Silva, G. de Oliveira Santiago Santos, M.M. de Salles Pupo, K.I.B. Eguiluz, G.R. Salazar-Banda, Influence of heating rate on the physical and electrochemical properties of mixed metal oxides anodes synthesized by thermal decomposition method applying an ionic liquid, J. Electroanal. Chem. 813 (2018) 127–133, https://doi.org/10.1016/j.jelechem.2018.02.026.

[42] A.R. Dória, G.O.S. Santos, M.M.S. Pelegrinelli, D.C. Silva, D.B. de Matos, E. B. Cavalcanti, R.S. Silva, G.R. Salazar-Banda, K.I.B. Eguiluz, Improved 4-nitrophenol removal at Ti/RuO_2–Sb_2O_4–TiO_2 laser-made anodes, Environ. Sci. Pollut. Res. 28 (2021) 23634–23646, https://doi.org/10.1007/s11356-020-10451-6.

[43] L. Wan, J.F. Li, J.Y. Feng, W. Sun, Z.Q. Mao, Anatase TiO_2 films with 2.2 eV band gap prepared by micro-arc oxidation, Mater. Sci. Eng. B Solid-State Mater. Adv. Technol. 139 (2007) 216–220, https://doi.org/10.1016/j.mseb.2007.02.014.

[44] E. Morais, C. O'Modhrain, K.R. Thampi, J.A. Sullivan, RuO_2/TiO_2 photocatalysts prepared via a hydrothermal route: Influence of the presence of TiO_2 on the reactivity of RuO_2 in the artificial photosynthesis reaction, J. Catal. 401 (2021) 288–296, https://doi.org/10.1016/j.jcat.2021.08.007.

[45] R.D. Coteiro, F.S. Teruel, J. Ribeiro, A.R.De Andrade, Effect of solvent on the preparation and characterization of DSA®-type anodes containing RuO_2-TiO_2-SnO_2, J. Braz. Chem. Soc. 17 (2006) 771–779, https://doi.org/10.1590/S0103-50532006000400020.

[46] S.M. Lin, T.C. Wen, A mixture design approach to the service life and the oxygen evolving catalytic activity of Ru-Sn-Ti ternary oxide coated electrodes, J. Appl. Electrochem 23 (1993) 487–494, https://doi.org/10.1007/BF00707627.

[47] P. Shrivastava, M.S. Moats, Wet film application techniques and their effects on the stability of RuO_2-TiO_2 coated titanium anodes, J. Appl. Electrochem 39 (2009) 107–116, https://doi.org/10.1007/s10800-008-9643-y.

[48] F. Moradi, C. Dehghanian, Addition of IrO_2 to RuO_2+TiO_2 coated anodes and its effect on electrochemical performance of anodes in acid media, Prog. Nat. Sci. Mater. Int 24 (2014) 134–141, https://doi.org/10.1016/j.pnsc.2014.03.008.

[49] J.J.S. Teles, E.R. Faria, D.V. Franco, L.M. da Silva, Inner and outer surface areas, electrochemical porosity, and morphology factor of mixed oxide-covered mesh electrodes with a nominal composition of MOME-$Sn_{0.5}Ir_xRu_{(0.5-x)}O_2$, Int. J. Electrochem. Sci. 12 (2017) 1755–1773, https://doi.org/10.20964/2017.03.34.

[50] G.O.S. Santos, V.M. Vasconcelos, R.S. da Silva, M.A. Rodrigo, K.I.B. Eguiluz, G. R. Salazar-Banda, New laser-based method for the synthesis of stable and active Ti/SnO_2–Sb anodes, Electrochim. Acta 332 (2020), https://doi.org/10.1016/j.electacta.2019.135478.

[51] G.R.P. Malpass, R.S. Neves, A.J. Motheo, A comparative study of commercial and laboratory-made Ti/$Ru_{0.3}Ti_{0.7}O_2$ DSA® electrodes: "In situ" and "ex situ" surface characterisation and organic oxidation activity, Electrochim. Acta 52 (2006) 936–944, https://doi.org/10.1016/j.electacta.2006.06.032.

[52] M. Lisker, T. Hur'yeva, Y. Ritterhaus, E.P. Burte, Effect of annealing in oxygen atmosphere on morphological and electrical properties of iridium and ruthenium thin films prepared by liquid delivery MOCVD, Surf. Coat. Technol. 201 (2007) 9294–9298, https://doi.org/10.1016/j.surfcoat.2007.04.078.

[53] S.M. Hoseinieh, F. Ashrafizadeh, Influence of electrolyte composition on deactivation mechanism of a Ti/$Ru_{0.25}Ir_{0.25}Ti_{0.50}O_2$ electrode, Ion. (Kiel.) 19 (2013) 113–125, https://doi.org/10.1007/s11581-012-0737-5.

[54] G. Divyapriya, S. Singh, C.A. Martínez-Huitle, J. Scaria, A.V. Karim, P.V. Nidheesh, Treatment of real wastewater by photoelectrochemical methods: an overview, Chemosphere 276 (2021), 130188, https://doi.org/10.1016/j.chemosphere.2021.130188.

[55] R. Antonelli, G.R.P. Malpass, M.G. Carlos da Silva, M.G.A. Vieira, Ofloxacin degradation in chloride-containing medium by photo-assisted sonoelectrochemical process using a mixed metal oxide anode, J. Environ. Chem. Eng. 10 (2022), 107174, https://doi.org/10.1016/j.jece.2022.107174.

[56] D.C. De Moura, C.K.C. De Araújo, C.L.P.S. Zanta, R. Salazar, C.A. Martínez-Huitle, Active chlorine species electrogenerated on Ti/$Ru_{0.3}Ti_{0.7}O_2$ surface: electrochemical behavior, concentration determination and their application, J. Electroanal. Chem. 731 (2014) 145–152, https://doi.org/10.1016/j.jelechem.2014.08.008.

[57] G. de, O.S. Santos, K.I.B. Eguiluz, G.R. Salazar-Banda, C. Saez, M.A. Rodrigo, Photoelectrolysis of clopyralid wastes with a novel laser-prepared MMO-RuO_2TiO_2 anode, Chemosphere 244 (2020), 125455, https://doi.org/10.1016/j.chemosphere.2019.125455.

[58] G. Hurwitz, P. Pornwongthong, S. Mahendra, E.M.V. Hoek, Degradation of phenol by synergistic chlorine-enhanced photo-assisted electrochemical oxidation, Chem. Eng. J. 240 (2014) 235–243, https://doi.org/10.1016/j.cej.2013.11.087.

[59] I.J.S. Montes, B.F. Silva, J.M. Aquino, On the performance of a hybrid process to mineralize the herbicide tebuthiuron using a DSA® anode and UVC light: a mechanistic study, Appl. Catal. B Environ. 200 (2017) 237–245, https://doi.org/10.1016/j.apcatb.2016.07.003.

[60] M.J.M. de Vidales, C. Sáez, J.F. Pérez, S. Cotillas, J. Llanos, P. Cañizares, M. A. Rodrigo, Irradiation-assisted electrochemical processes for the removal of persistent organic pollutants from wastewater, J. Appl. Electrochem 45 (2015) 799–808, https://doi.org/10.1007/s10800-015-0825-0.

[61] I. Sánchez-Montes, J.F. Pérez, C. Sáez, M.A. Rodrigo, P. Cañizares, J.M. Aquino, Assessing the performance of electrochemical oxidation using DSA® and BDD anodes in the presence of UVC light, Chemosphere 238 (2020), https://doi.org/10.1016/j.chemosphere.2019.124575.

[62] Y. Mu, C. Huang, H. Li, L. Chen, D. Zhang, Z. Yang, Electrochemical degradation of ciprofloxacin with a Sb-doped SnO_2 electrode: performance, influencing factors and degradation pathways, RSC Adv. 9 (2019) 29796–29804, https://doi.org/10.1039/c9ra04860j.

[63] G. Li, S. Zhou, Z. Shi, X. Meng, L. Li, B. Liu, Electrochemical degradation of ciprofloxacin on BDD anode using a differential column batch reactor: mechanisms, kinetics and pathways, Environ. Sci. Pollut. Res. 26 (2019) 17740–17750, https://doi.org/10.1007/s11356-019-04900-0.

[64] Y. Wang, C. Shen, M. Zhang, B.T. Zhang, Y.G. Yu, The electrochemical degradation of ciprofloxacin using a SnO_2-Sb/Ti anode: Influencing factors, reaction pathways and energy demand, Chem. Eng. J. 296 (2016) 79–89, https://doi.org/10.1016/j.cej.2016.03.093.

[65] R.E. Palma-Goyes, J. Vazquez-Arenas, C. Ostos, F. Ferraro, R.A. Torres-Palma, I. Gonzalez, Microstructural and electrochemical analysis of Sb_2O_5 doped-Ti/RuO_2-ZrO_2 to yield active chlorine species for ciprofloxacin degradation, Electrochim. Acta 213 (2016) 740–751, https://doi.org/10.1016/j.electacta.2016.07.150.